Measurement of α_s from Jet Rates in Deep Inelastic Scattering at HERA

ZEUS Collaboration

hep-ex/9510001   8 Oct 1995

Abstract

Jet production in deep inelastic scattering for $120 < Q^2 < 3600$ GeV^2 has been studied using data from an integrated luminosity of 3.2 pb^{-1} collected with the ZEUS detector at HERA. Jets are identified with the JADE algorithm. A cut on the angular distribution of parton emission in the γ^*-parton centre-of-mass system minimises the experimental and theoretical uncertainties in the determination of the jet rates. The jet rates, when compared to $\mathcal{O}(\alpha_s{}^2)$ perturbative QCD calculations, allow a precise determination of $\alpha_s(Q)$ in three Q^2-intervals. The values are consistent with a running of $\alpha_s(Q)$, as expected from QCD. Extrapolating to $Q = M_{Z^0}$ yields $\alpha_s(M_{Z^0}) = 0.117 \pm 0.005\ (stat)\ ^{+0.004}_{-0.005}\ (syst_{exp})\ \pm 0.007\ (syst_{theory})$.

The ZEUS Collaboration

M. Derrick, D. Krakauer, S. Magill, D. Mikunas, B. Musgrave, J. Repond, R. Stanek, R.L. Talaga, H. Zhang
Argonne National Laboratory, Argonne, IL, USA [p]

R. Ayad[1], G. Bari, M. Basile, L. Bellagamba, D. Boscherini, A. Bruni, G. Bruni, P. Bruni, G. Cara Romeo,
G. Castellini[2], M. Chiarini, L. Cifarelli[3], F. Cindolo, A. Contin, M. Corradi, I. Gialas[4], P. Giusti, G. Iacobucci,
G. Laurenti, G. Levi, A. Margotti, T. Massam, R. Nania, C. Nemoz,
F. Palmonari, A. Polini, G. Sartorelli, R. Timellini, Y. Zamora Garcia[1], A. Zichichi
University and INFN Bologna, Bologna, Italy [f]

A. Bargende[5], A. Bornheim, J. Crittenden, K. Desch, B. Diekmann[6], T. Doeker, M. Eckert, L. Feld, A. Frey,
M. Geerts, M. Grothe, H. Hartmann, K. Heinloth, E. Hilger, H.-P. Jakob, U.F. Katz,
S. Mengel, J. Mollen, E. Paul, M. Pfeiffer, Ch. Rembser, D. Schramm, J. Stamm, R. Wedemeyer
Physikalisches Institut der Universität Bonn, Bonn, Germany [c]

S. Campbell-Robson, A. Cassidy, W.N. Cottingham, N. Dyce, B. Foster, S. George, M.E. Hayes, G.P. Heath,
H.F. Heath, C.J.S. Morgado, J.A. O'Mara, D. Piccioni, D.G. Roff, R.J. Tapper, R. Yoshida
H.H. Wills Physics Laboratory, University of Bristol, Bristol, U.K. [o]

R.R. Rau
Brookhaven National Laboratory, Upton, L.I., USA [p]

M. Arneodo[7], M. Capua, A. Garfagnini, L. Iannotti, M. Schioppa, G. Susinno
Calabria University, Physics Dept.and INFN, Cosenza, Italy [f]

A. Bernstein, A. Caldwell[8], N. Cartiglia, J.A. Parsons, S. Ritz[9], F. Sciulli, P.B. Straub, L. Wai, S. Yang, Q. Zhu
Columbia University, Nevis Labs., Irvington on Hudson, N.Y., USA [q]

P. Borzemski, J. Chwastowski, A. Eskreys, K. Piotrzkowski, M. Zachara, L. Zawiejski
Inst. of Nuclear Physics, Cracow, Poland [j]

L. Adamczyk, B. Bednarek, K. Jeleń, D. Kisielewska, T. Kowalski, E. Rulikowska-Zarębska,
L. Suszycki, J. Zając
Faculty of Physics and Nuclear Techniques, Academy of Mining and Metallurgy, Cracow, Poland [j]

A. Kotański, M. Przybycień
Jagellonian Univ., Dept. of Physics, Cracow, Poland [k]

L.A.T. Bauerdick, U. Behrens, H. Beier[10], J.K. Bienlein, C. Coldewey, O. Deppe, K. Desler, G. Drews,
M. Flasiński[11], D.J. Gilkinson, C. Glasman, P. Göttlicher, J. Große-Knetter, B. Gutjahr[12], T. Haas, W. Hain,
D. Hasell, H. Heßling, Y. Iga, K.F. Johnson[13], P. Joos, M. Kasemann, R. Klanner, W. Koch, L. Köpke[14],
U. Kötz, H. Kowalski, J. Labs, A. Ladage, B. Löhr, M. Löwe, D. Lüke, J. Mainusch, O. Mańczak, T. Monteiro[15],
J.S.T. Ng, S. Nickel[16], D. Notz, K. Ohrenberg, M. Roco, M. Rohde, J. Roldán, U. Schneekloth, W. Schulz,
F. Selonke, E. Stiliaris[17], B. Surrow, T. Voß, D. Westphal, G. Wolf, C. Youngman, W. Zeuner, J.F. Zhou[18]
Deutsches Elektronen-Synchrotron DESY, Hamburg, Germany

H.J. Grabosch, A. Kharchilava[19], A. Leich, M.C.K. Mattingly[20], S.M. Mari[4], A. Meyer,
S. Schlenstedt, N. Wulff
DESY-Zeuthen, Inst. für Hochenergiephysik, Zeuthen, Germany

G. Barbagli, P. Pelfer
University and INFN, Florence, Italy [f]

G. Anzivino, G. Maccarrone, S. De Pasquale, L. Votano
INFN, Laboratori Nazionali di Frascati, Frascati, Italy [f]

A. Bamberger, S. Eisenhardt, A. Freidhof, S. Söldner-Rembold[21], J. Schroeder[22], T. Trefzger
Fakultät für Physik der Universität Freiburg i.Br., Freiburg i.Br., Germany [c]

N.H. Brook, P.J. Bussey, A.T. Doyle[23], D.H. Saxon, M.L. Utley, A.S. Wilson
Dept. of Physics and Astronomy, University of Glasgow, Glasgow, U.K. [o]

A. Dannemann, U. Holm, D. Horstmann, T. Neumann, R. Sinkus, K. Wick
Hamburg University, I. Institute of Exp. Physics, Hamburg, Germany [c]

E. Badura[24], B.D. Burow[25], L. Hagge[26], E. Lohrmann, J. Milewski, M. Nakahata[27], N. Pavel, G. Poelz,
W. Schott, F. Zetsche
Hamburg University, II. Institute of Exp. Physics, Hamburg, Germany [c]

T.C. Bacon, N. Bruemmer, I. Butterworth, E. Gallo, V.L. Harris, B.Y.H. Hung, K.R. Long, D.B. Miller,
P.P.O. Morawitz, A. Prinias, J.K. Sedgbeer, A.F. Whitfield
Imperial College London, High Energy Nuclear Physics Group, London, U.K. [o]

U. Mallik, E. McCliment, M.Z. Wang, S.M. Wang, J.T. Wu
University of Iowa, Physics and Astronomy Dept., Iowa City, USA [p]

P. Cloth, D. Filges
Forschungszentrum Jülich, Institut für Kernphysik, Jülich, Germany

S.H. An, S.M. Hong, S.W. Nam, S.K. Park, M.H. Suh, S.H. Yon
Korea University, Seoul, Korea [h]

R. Imlay, S. Kartik, H.-J. Kim, R.R. McNeil, W. Metcalf, V.K. Nadendla
Louisiana State University, Dept. of Physics and Astronomy, Baton Rouge, LA, USA [p]

F. Barreiro[28], G. Cases, J.P. Fernandez, R. Graciani, J.M. Hernández, L. Hervás[28], L. Labarga[28], M. Martinez,
J. del Peso, J. Puga, J. Terron, J.F. de Trocóniz
Univer. Autónoma Madrid, Depto de Física Teoríca, Madrid, Spain [n]

G.R. Smith
University of Manitoba, Dept. of Physics, Winnipeg, Manitoba, Canada [a]

F. Corriveau, D.S. Hanna, J. Hartmann, L.W. Hung, J.N. Lim, C.G. Matthews, P.M. Patel,
L.E. Sinclair, D.G. Stairs, M. St.Laurent, R. Ullmann, G. Zacek
McGill University, Dept. of Physics, Montréal, Québec, Canada [a, b]

V. Bashkirov, B.A. Dolgoshein, A. Stifutkin
Moscow Engineering Physics Institute, Mosocw, Russia [l]

G.L. Bashindzhagyan[23], P.F. Ermolov, L.K. Gladilin, Yu.A. Golubkov, V.D. Kobrin,
I.A. Korzhavina, V.A. Kuzmin, O.Yu. Lukina, A.S. Proskuryakov, A.A. Savin, L.M. Shcheglova,
A.N. Solomin, N.P. Zotov
Moscow State University, Institute of Nuclear Physics, Moscow, Russia [m]

M. Botje, F. Chlebana, A. Dake, J. Engelen, M. de Kamps, P. Kooijman, A. Kruse, H. Tiecke, W. Verkerke,
M. Vreeswijk, L. Wiggers, E. de Wolf, R. van Woudenberg
NIKHEF and University of Amsterdam, Netherlands [i]

D. Acosta, B. Bylsma, L.S. Durkin, J. Gilmore, K. Honscheid, C. Li, T.Y. Ling, K.W. McLean[29], W.N. Murray,
P. Nylander, I.H. Park, T.A. Romanowski[30], R. Seidlein[31]
Ohio State University, Physics Department, Columbus, Ohio, USA [p]

D.S. Bailey, A. Byrne[32], R.J. Cashmore, A.M. Cooper-Sarkar, R.C.E. Devenish, N. Harnew,
M. Lancaster, L. Lindemann[4], J.D. McFall, C. Nath, V.A. Noyes, A. Quadt, J.R. Tickner,
H. Uijterwaal, R. Walczak, D.S. Waters, F.F. Wilson, T. Yip
Department of Physics, University of Oxford, Oxford, U.K. [o]

G. Abbiendi, A. Bertolin, R. Brugnera, R. Carlin, F. Dal Corso, M. De Giorgi, U. Dosselli,
S. Limentani, M. Morandin, M. Posocco, L. Stanco, R. Stroili, C. Voci
Dipartimento di Fisica dell' Universita and INFN, Padova, Italy [f]

II

J. Bulmahn, J.M. Butterworth, R.G. Feild, B.Y. Oh, J.R. Okrasinski[33], J.J. Whitmore[34]
Pennsylvania State University, Dept. of Physics, University Park, PA, USA [q]

G. D'Agostini, G. Marini, A. Nigro, E. Tassi
Dipartimento di Fisica, Univ. 'La Sapienza' and INFN, Rome, Italy [f]

J.C. Hart, N.A. McCubbin, K. Prytz, T.P. Shah, T.L. Short
Rutherford Appleton Laboratory, Chilton, Didcot, Oxon, U.K. [o]

E. Barberis, T. Dubbs, C. Heusch, M. Van Hook, W. Lockman, J.T. Rahn, H.F.-W. Sadrozinski, A. Seiden,
D.C. Williams
University of California, Santa Cruz, CA, USA [p]

J. Biltzinger, R.J. Seifert, O. Schwarzer, A.H. Walenta, G. Zech
Fachbereich Physik der Universität-Gesamthochschule Siegen, Germany [c]

H. Abramowicz, G. Briskin, S. Dagan[35], C. Händel-Pikielny, A. Levy[23]
School of Physics,Tel-Aviv University, Tel Aviv, Israel [e]

J.I. Fleck, T. Hasegawa, M. Hazumi, T. Ishii, M. Kuze, S. Mine, Y. Nagasawa, M. Nakao, I. Suzuki, K. Tokushuku,
S. Yamada, Y. Yamazaki
Institute for Nuclear Study, University of Tokyo, Tokyo, Japan [g]

M. Chiba, R. Hamatsu, T. Hirose, K. Homma, S. Kitamura, Y. Nakamitsu, K. Yamauchi
Tokyo Metropolitan University, Dept. of Physics, Tokyo, Japan [g]

R. Cirio, M. Costa, M.I. Ferrero, L. Lamberti, S. Maselli, C. Peroni, R. Sacchi, A. Solano, A. Staiano
Universita di Torino, Dipartimento di Fisica Sperimentale and INFN, Torino, Italy [f]

M. Dardo
II Faculty of Sciences, Torino University and INFN - Alessandria, Italy [f]

D.C. Bailey, D. Bandyopadhyay, F. Benard, M. Brkic, D.M. Gingrich[36], G.F. Hartner, K.K. Joo, G.M. Levman,
J.F. Martin, R.S. Orr, S. Polenz, C.R. Sampson, R.J. Teuscher
University of Toronto, Dept. of Physics, Toronto, Ont., Canada [a]

C.D. Catterall, T.W. Jones, P.B. Kaziewicz, J.B. Lane, R.L. Saunders, J. Shulman
University College London, Physics and Astronomy Dept., London, U.K. [o]

K. Blankenship, B. Lu, L.W. Mo
Virginia Polytechnic Inst. and State University, Physics Dept., Blacksburg, VA, USA [q]

W. Bogusz, K. Charchuła, J. Ciborowski, J. Gajewski, G. Grzelak[37], M. Kasprzak, M. Krzyżanowski,
K. Muchorowski[38], R.J. Nowak, J.M. Pawlak, T. Tymieniecka, A.K. Wróblewski, J.A. Zakrzewski, A.F. Żarnecki
Warsaw University, Institute of Experimental Physics, Warsaw, Poland [j]

M. Adamus
Institute for Nuclear Studies, Warsaw, Poland [j]

Y. Eisenberg[35], U. Karshon[35], D. Revel[35], D. Zer-Zion
Weizmann Institute, Nuclear Physics Dept., Rehovot, Israel [d]

I. Ali, W.F. Badgett, B. Behrens, S. Dasu, C. Fordham, C. Foudas, A. Goussiou, R.J. Loveless, D.D. Reeder,
S. Silverstein, W.H. Smith, A. Vaiciulis, M. Wodarczyk
University of Wisconsin, Dept. of Physics, Madison, WI, USA [p]

T. Tsurugai
Meiji Gakuin University, Faculty of General Education, Yokohama, Japan

S. Bhadra, M.L. Cardy, C.-P. Fagerstroem, W.R. Frisken, K.M. Furutani, M. Khakzad, W.B. Schmidke
York University, Dept. of Physics, North York, Ont., Canada [a]

1 Introduction

Neutral current (NC) deep inelastic scattering (DIS) ($lp \rightarrow lX; l = e, \mu$), is characterised by the exchange of a virtual photon or Z^0 boson between the incident lepton and proton. In the naive quark-parton-model (QPM) the process $V^*q \rightarrow q$ ($V = \gamma, Z^0$) gives rise to 1+1 jets in the final state corresponding to the struck quark from the proton and the proton remnant (hereafter denoted by "+1"). Multi-jet production in DIS beyond 1+1 jets provides a good laboratory for testing quantum chromodynamics (QCD). From the measured rate of 2+1 jet events it is possible to determine the strong coupling constant α_s, for fixed kinematics and a given jet definition, by comparing to theoretical calculations in which α_s is the only free parameter.

To leading order in α_s, 2+1 jet production proceeds via QCD-Compton scattering ($V^*q \rightarrow qg$) and boson-gluon fusion (BGF) ($V^*g \rightarrow q\overline{q}$). For the extraction of α_s from the measured jet rates to be reliable the 2+1 jet rate must be calculated at least to next-to-leading order (NLO) in QCD, where the renormalisation scheme is defined unambiguously. Furthermore the jet definition has to be treated in the same way in theory and experiment for a quantitative comparison with the predictions of QCD. Theoretical calculations [1, 2, 3, 4] for the jet rates at the parton level are currently available only for the JADE jet definition scheme [5]. Therefore the measured jet rates, obtained using the same jet-finding scheme, have to be corrected to the parton level so that a comparison with the NLO $\mathcal{O}(\alpha_s{}^2)$ calculations can be made in order to determine α_s. The extracted α_s value can be expected to be reliable when the NLO calculations reproduce the corrected jet rates over a wide kinematic range and the extracted value is insensitive to the cuts applied at the detector level. In this analysis a cut on the parton variable z (described later) is applied, which restricts the phase space so that these requirements are well satisfied.

Multi-jet production in DIS has been studied by the E665 fixed-target experiment at FERMILAB at a low centre-of-mass energy, $\sqrt{s}$, of ~ 30 GeV [6], and at higher energies, $\sqrt{s}$=300 GeV, by ZEUS [7] and H1 [8] at HERA where jet structures are more clearly discernible. This paper describes the extraction of α_s from measurements of multi-jet rates at Q^2 between 120 and 3600 GeV^2. An earlier study of jet rates and jet kinematics has been reported by this experiment [9]; an extraction of α_s from multi-jet production has been reported by H1 [10].

2 The ZEUS Detector

The data used in this analysis were collected with the ZEUS detector during 1994 when HERA provided collisions between 27.5 GeV electrons or positrons[1] and 820 GeV protons, yielding a centre-of-mass energy of 300 GeV. They correspond to an integrated luminosity of 3.2 pb^{-1}.

ZEUS is an almost hermetic, multipurpose, magnetic detector and has been described elsewhere in detail [11]. Here a brief description of the components relevant for this analysis is given. Charged particles are tracked by the inner tracking detectors which operate in a magnetic field of 1.43 T provided by a thin superconducting coil. Immediately surrounding the beam pipe is the vertex detector, a drift chamber, which consists of 120 radial cells, each with 12 sense wires [12]. It is surrounded by the central tracking detector which consists of 72 cylindrical

---

[1]Hereafter "electron" is used in a generic sense to refer to e^- or e^+.

drift chamber layers, organised into 9 'superlayers' [13]. In the present analysis these tracking detectors are primarily used for the determination of the event vertex.

The energy associated with the hadronic final state and the scattered electron is measured with the uranium-scintillator calorimeter (CAL) [14] which consists of three parts: the forward (FCAL), the rear (RCAL) and the barrel calorimeter (BCAL).The ZEUS coordinate system is defined as right handed with the Z axis pointing in the proton beam direction, hereafter referred to as "forward". The X axis points horizontally towards the centre of HERA and the Y axis points vertically upwards. The polar angle θ is defined with respect to the Z direction. Each part of the calorimeter is subdivided longitudinally into one electromagnetic section (EMC) and one hadronic section (HAC) for the RCAL and two HAC sections for BCAL and FCAL. Holes of 20×20 cm^2 at the centre of FCAL and RCAL accommodate the HERA beam pipe. In the XY plane around the FCAL beam pipe, the HAC section is segmented in 20×20 cm^2 cells and the EMC section in 5×20 cm^2 cells. In total, the calorimeter consists of approximately 6000 cells. In terms of pseudorapidity, $\eta = -\ln \tan \frac{\theta}{2}$, the FCAL covers the interval $4.3 \geq \eta \geq 1.1$, the BCAL $1.1 \geq \eta \geq -0.75$ and the RCAL $-0.75 \geq \eta \geq -3.8$, for the nominal interaction point at $X = Y = Z = 0$. The CAL energy resolution, as measured under test beam conditions, is $\sigma_E/E = 0.18/\sqrt{E}$ for electrons and $\sigma_E/E = 0.35/\sqrt{E}$ for hadrons (E in GeV). The time resolution of the calorimeter, which is important for rejecting beam-gas backgrounds, is better than 1 ns for energy deposits greater than 4.5 GeV.

3 Event Kinematics

For a given ep centre-of-mass energy $\sqrt{s}$, the differential cross section for leading order $\mathcal{O}(\alpha_s{}^1)$ 2+1 jet production in DIS depends on 5 independent kinematic variables, which we take as x, y, x_p, z, and Φ [15]. The first two, Bjorken-x and y, are sufficient to describe the $\mathcal{O}(\alpha_s{}^0)$ QPM 1+1 jet process. They correspond to the momentum fraction of the proton carried by the struck quark (x) and the fractional energy transfer between the electron and the proton in the proton rest frame (y). Three additional variables (x_p, z, Φ) are introduced to describe the 2+1 parton kinematics. The parton variable x_p is defined by:

$$x_p = \frac{Q^2}{2\, p \cdot q} = \frac{Q^2}{Q^2 + m_{ij}^2} = \frac{x}{\xi},$$

where q is the four-momentum of the exchanged virtual boson in the ep scattering process, ξ is the fraction of the proton's four-momentum P carried by the incoming parton with four-momentum $p = \xi P$, m_{ij} is the invariant mass of the two non-remnant jets and $Q^2 = -q^2$. Q^2, x and y are related by $Q^2 = s\, x\, y$. The parton variable z is defined by:

$$z_1 = \frac{p \cdot p_1}{p \cdot q} = \frac{1}{2} \cdot (1 - \cos \theta_1^*) = \frac{E_1 \cdot (1 - \cos \theta_1)}{\sum_{i=1,2} E_i \cdot (1 - \cos \theta_i)}.$$

The formula is given for one of the partons $i = 1$. The outgoing four-momentum of the parton from the hard scattering is p_1 and θ_1^* is the scattering angle in the γ^*-parton centre-of-mass system. Experimentally, z is determined in the HERA system from the energies and angles, E_i and θ_i, of the two jets. The jets are assumed to be massless. The other parton satisfies the constraint $z_2 = 1 - z_1$. The angle Φ represents the azimuthal angle between the parton and lepton scattering planes in the γ^*-parton centre-of-mass system.

Since the ZEUS detector is nearly hermetic, it is possible to reconstruct the kinematic variables x, y and Q^2 for NC DIS using different combinations of the angles and energies of the scattered lepton and of the hadronic system [16]. The electron method was used to determine y as y_e from E'_e and θ_e, the energy and polar angle of the scattered electron. The hadronic, or Jacquet-Blondel method [17], was used to reconstruct y as $y_{JB} = \sum_h E_h(1 - cos\theta_h)/(2E_e)$ where E_h and θ_h are the energy and polar angle calculated from the calorimeter cells not associated with the scattered electron, and E_e is the electron beam energy. The double angle (DA) method uses θ_e and γ_H, the polar angle of the struck quark in the QPM which is given by $\cos \gamma_H = (\sum_h p_{T,h}^2 - (2E_e y_{JB})^2)/(\sum_h p_{T,h}^2 + (2E_e y_{JB})^2)$. The DA method, which measures Q^2 with small bias and good resolution in the kinematic range of this analysis, was used to reconstruct the x, y and Q^2 variables of NC events (and the jet variables x_p and z defined above) [16].

4   Trigger Conditions and Event Selection

The trigger and event selection followed closely that described in reference [9]. The trigger acceptance was essentially independent of the hadronic final state with an acceptance greater than 97 % for $Q^2 > 10$ GeV^2. Neutral current DIS events were selected by the following criteria: the event times measured by the FCAL and the RCAL had to be consistent with an interaction inside the detector. This cut strongly reduced beam-gas background. The Z position of the event vertex was reconstructed from the tracking data. Events were accepted if the Z position was within ± 50 cm of the nominal interaction point. An electron candidate with energy greater than 10 GeV had to be found in the calorimeter. To reject backgrounds from photoproduction events with a fake electron (mostly π^0's close to the proton beam) the electron candidate was required to satisfy $y_e < 0.95$. Photoproduction and beam-gas backgrounds were further suppressed by demanding energy-momentum conservation. For a fully contained event, and neglecting the detector resolution, one expects $E - P_Z = 2 \cdot E_e$, where E and P_Z are the summed energy and Z-component of the momenta of all objects measured in the calorimeter. Taking the detector resolution into account 35 GeV$< E - P_Z < 60$ GeV was required to select DIS events. The background from photoproduction was estimated to be negligible and that from QED Compton scattering was found to be less than 1%. Diffractive events, which do not deposit a significant amount of energy in the FCAL, did not pass the selection criteria given below. Finally, beam halo muons and cosmic rays were rejected by suitable algorithms.

Several considerations motivated the selection of the kinematic region used for the α_s measurement. First, the analysis was restricted to high Q^2, where clear jet structures are observed and hadronisation uncertainties are minimised. Secondly, theoretical uncertainties in the 2+1 jet cross section are small at high x, where the parton densities of the proton are well known. In addition at high x the uncertainty stemming from the initial state parton-showers, used in the Monte Carlo simulation to correct the data to the partonic level, was reduced. Thirdly, the acceptance for 2+1 jet events increases at high y: in particular, the forward jet is well contained within the detector. Finally, all of the above concerns were balanced against the need for sufficient statistics. The kinematic region selected for the final analysis was therefore: $120 < Q^2 < 3600$ GeV^2, $0.01 < x < 0.1$, and $0.1 < y < 0.95$, resulting in a sample of 4472 events. The Q^2 range was further subdivided into three regions to measure $\alpha_s(Q)$ at increasing scales as a consistency check and as a test for the running of the strong coupling constant.

These ranges were: $120 < Q^2 < 240$, $240 < Q^2 < 720$, and $720 < Q^2 < 3600$ GeV^2. The number of events in each region were 1649, 2048 and 775, respectively.

5 Jet Definition and Jet Kinematics

The JADE algorithm [5] was used to relate the hadronic final state measured in the detector to the underlying hard scattering processes. It is a cluster algorithm based on the scaled invariant mass, $y_{ij} = m_{ij}^2/W^2 = 2E_iE_j(1 - cos\theta_{ij})/W^2$, where m_{ij} is the invariant mass of the two objects i and j, which are assumed to be massless. The scale W^2 is the squared invariant mass of the overall hadronic final state and E_i, E_j and θ_{ij} are the energies of the objects and the angle between them. Starting with the minimum y_{ij} of all possible combinations, objects were merged by adding their four-momenta until y_{ij} for all objects exceeded a jet resolution parameter y_{cut}. Those objects remaining were then considered as jets. The JADE algorithm was slightly modified [18, 19] for use at the detector level in ep collisions by the addition of a pseudo-particle inserted along the Z axis. The missing longitudinal momentum in each event was assigned to the momentum of the pseudo-particle. It prevents the detected fraction of particles originating from the proton remnant from forming spurious jets.

The measured calorimeter energies above 150 (200) MeV for EMC (HAC) cells and their angles relative to the interaction point were used to define vectors which were input to the JADE algorithm in the detector level analysis. At the detector level, the scale W was calculated as $W_{vis}^2 = s\,(1 - x_{DA})\,y_{JB}$. This value reflects the measured rather than the true hadronic activity and so reduces the event-by-event correction for the detector resolution when calculating y_{ij}.

For 2+1 jet production in DIS, one of the non-remnant jets is typically directed forward because of the forward singularity in the cross section. Such forward singularities are regulated in the theory by the cutoff y_{cut}. Requiring a large y_{cut} is, however, not sufficient to avoid the problems arising from forward-going jets close to the beam pipe and the proton remnant. This is achieved by a cut on the parton variable, z, for 2+1 jet events[2]. In QCD the rapid rise towards $z = 0$ results from collinear and infrared singularities. In order to avoid this kinematical region the analysis was restricted to events satisfying $0.1 < z < 0.9$. This requirement also reduces the fraction of forward jets ($\theta_{jet} < 8°$) from 30% to 10%. Figure 1a shows the dR_{2+1}/dz distribution for 2+1 jet events. Here $R_{j+1} = N_{j+1}/N_{tot}$, where j stands for 0, 1, 2, or 3, N_{j+1} is the number of (j+1) jet events and N_{tot} is the total number of selected DIS events. Figures 1b–d show the resulting x_p, p_T and m_{ij} distributions. The predictions of the NLO calculations of DISJET and PROJET (discussed later) are also shown in Fig. 1. The z-cut results in a significantly improved agreement between the calculations and the data compared to our earlier analysis done without this restriction on z [9]. This cut removes jets with transverse momenta p_T below ~ 4 GeV where p_T is measured with respect to the γ^* direction and is calculated in the γ^*-parton system as:

$$p_T = \sqrt{Q^2 \cdot \frac{1}{x_p} \cdot (1 - x_p) \cdot z\,(1 - z)}.$$

---

[2]z is not defined for 1+1 and 3+1 jet events. In the following, 2+1 jet events failing to pass the z cut are not considered as 2+1 jet events. 1+1 and 3+1 jet events are counted in N_{tot}, the total number of selected events.

6   Jet Reconstruction and Jet Rates

The acceptance and resolution, as well as the correction of the measured jet rates to the parton level, were determined using Monte Carlo methods. Neutral current DIS events, generated using LEPTO 6.1 [20] and the Lund string fragmentation model [21] for the hadronisation, were interfaced via DJANGO6 2.1 [22] to HERACLES 4.1 [23] for QED radiative corrections. They were passed through a GEANT [24] based detector simulation, and subsequently analysed with the same reconstruction, selection and jet analysis procedures as the data. Both the hard emission of partons at the matrix element level (calculated to leading order in α_s) and the higher order soft parton showers are included in the LEPTO matrix element, parton shower (MEPS) model. The MEPS model satisfactorily describes the global jet properties and production rates observed for the data in the selected kinematic region [9].

When generating events with the MEPS model, default values of all parameters were used except for the parameter y_{min}, which sets a minimum y_{ij} of partons in first order QCD matrix elements [20]. The value of y_{min} was lowered from 0.015 to 0.005 in order to study the measured jet rate as a function of the jet resolution parameter y_{cut} for $y_{cut} >0.01$. The parton densities of the proton were taken from the MRSD′- set [25].

The jets were reconstructed by applying the JADE algorithm at the parton level, the hadron level and the detector level. These jets were constructed respectively from the output of the parton shower step of the event generator, the true momenta of the hadrons before the detector simulation and the energy deposits in the calorimeter cells after the detector simulation. The ratio of the jet rates at the different levels of the event simulation are the corresponding correction factors for hadronisation (C_h) and detector simulation (C_d), with which the measured jet rates were multiplied. Both the detector and hadronisation corrections were found to be below 20%. Table 1 shows the correction factors and the corrected jet rates R_{2+1} for the three Q^2 intervals and for the combined Q^2 region.

y_{cut}	$120 < Q^2 < 240$ (GeV ^{2})			$240 < Q^2 < 720$ (GeV ^{2})			$720 < Q^2 < 3600$ (GeV ^{2})			$120 < Q^2 < 3600$ (GeV ^{2})		
	R_{2+1}	C_d	C_h	R_{2+1}	C_d	C_h	R_{2+1}	C_d	C_h	R_{2+1}	C_d	C_h
0.010	12.1±0.9	1.02	1.04	13.5±0.9	0.92	1.04	11.5±1.3	0.88	1.03	12.6±0.6	0.94	1.05
0.015	10.0±0.8	0.99	1.04	10.8±0.8	0.96	1.05	9.3±1.2	0.89	1.02	10.4±0.5	0.96	1.05
0.020	7.8±0.7	0.96	1.05	9.0±0.7	0.96	1.05	8.6±1.1	0.92	1.01	8.6±0.5	0.96	1.05
0.030	5.3±0.6	0.92	1.10	6.5±0.5	0.98	1.08	6.7±1.0	0.95	1.05	6.2±0.5	0.96	1.08
0.040	4.1±0.6	0.93	1.13	4.6±0.5	0.96	1.10	4.6±0.8	0.94	1.06	4.4±0.4	0.96	1.08
0.050	3.3±0.5	1.02	1.16	3.6±0.5	0.99	1.11	3.9±0.8	0.93	1.07	3.5±0.3	0.99	1.10
0.060	2.3±0.4	0.94	1.20	2.7±0.3	1.02	1.15	2.9±0.7	0.92	1.07	2.6±0.2	0.99	1.13

Table 1: 2+1 jet production rates (in %) corrected to the parton level (R_{2+1}) and correction factors for detector effects (C_d) and for hadronisation (C_h) in the three Q^2 intervals and for the combined region. Errors shown are statistical only.

7 $\mathcal{O}(\alpha_s{}^2)$ Perturbative QCD Calculations

For NC electron-proton scattering, the 2+1 jet differential cross section at the $\mathcal{O}(\alpha_s{}^1)$ LO level, expressed in terms of the above variables, is given by:

$$\frac{d^2\sigma_{2+1}}{dx\,dy} = \frac{\alpha^2\,\alpha_s}{y\,Q^2} \cdot \int \frac{dx_p}{x_p} \int dz \int \frac{d\Phi}{2\pi}\,(I_g + I_q),$$

where I_g and I_q are the gluon- and quark-initiated contributions respectively [15] which contain singularities at $z = 0$, $z = 1$ and $x_p = 1$. The singularities correspond to the limit where two partons are irresolvable due to vanishing energy of one of the partons or vanishing opening angle. In the BGF process the singularity is related to the collinear emission of an outgoing quark in the proton remnant direction; for the QCD Compton process the singularity occurs when the momentum of the gluon is parallel to that of the quark or when the quark emits a very soft gluon. The integration must be done numerically because of the x-dependent parton density distributions. The integration limits for z and x_p in the JADE scheme are functions of the scaled invariant mass cutoff $y_{cut} = m_{ij}^2/W^2$, where W is the reference mass scale and m_{ij} is the invariant mass between any two partons [2]. Any pair of partons with a scaled invariant mass below this cutoff is not resolved. Therefore the singularities are regulated by a single cutoff parameter y_{cut}. The leading order (LO) and next-to-leading (NLO) order 2+1 jet cross section can be expressed as:

$$\frac{d\sigma_{2+1}^{LO}}{dx\,dy} = c_{31} \cdot \alpha_s,$$

$$\frac{d\sigma_{2+1}^{NLO}}{dx\,dy} = c_{31} \cdot \alpha_s + c_{32} \cdot \alpha_s^2.$$

Next-to-leading order corrections to $d\sigma_{2+1}$ include the contribution from unresolved 3+1 jet events as well as negative corrections coming from virtual loops [3, 4]. The coefficients c_{ij} contain the hard scattering matrix elements and the parton density functions of the incoming proton. The effect of a change in α_s on the parton densities is negligible for our Q^2 range [26]. The first index, i, stands for the jet multiplicity (including the remnant jet) and the second index, j, represents the order of the α_s calculation. After integrating over the jet variables (x_p, z, Φ) the coefficients c_{ij} are functions of the event kinematic variables x, y, y_{cut} and the factorisation scale μ_F; c_{32} depends also on the renormalisation scale μ_R [27]. The parton densities contained in c_{ij} are calculated at the scale Q^2. In finite order perturbative QCD calculations α_s depends on the renormalisation scale μ_R. The 2+1 jet rates are derived from the cross sections by $R_{2+1} = \sigma_{2+1}/\sigma_{tot}$. The resulting $\mathcal{O}(\alpha_s{}^2)$ corrections to R_{2+1}, using the NLO calculations, are considerable: they vary from –20 to +20% when y_{cut} is varied between 0.01 and 0.06 in the kinematic region used for this study [4, 3]. The numerical cross section calculations are available in the DISJET program [28] by Brodkorb and Mirkes, and in the PROJET program [29] by Graudenz. Both programs agree in their predictions of α_s for a given jet rate and they reproduce the shape of the measured jet rate distributions as a function of y_{cut} well in the investigated kinematic range (see below).

The renormalisation scheme used in the calculation is the $\overline{MS}$ scheme. In second order, the dependence on other renormalisation schemes can be completely specified by one parameter, which can be chosen to be the value of the renormalisation scale μ_R. We chose $\mu_R^2 = Q^2$ for

our analysis. The same scale is chosen for the factorisation scale μ_F. The parton densities were calculated with a fixed $\Lambda_{\overline{MS}}^{(5)} = 154$ MeV. In the kinematic range used in this analysis, the effect of varying $\Lambda_{\overline{MS}}$ in the parton densities is expected to be small [26]. In the programs the contributions from the $c-$ and $b-$quarks are zero in the parton density parametrisations below the single quark mass thresholds, as defined in the $\overline{MS}$ factorisation scheme. Above threshold, the contributions from the $c-$ and $b-$quarks are calculated assuming zero mass. The number of flavours in the formula for the running coupling constant is changed at the single mass threshold, as required by the $\overline{MS}$ renormalisation scheme, giving rise to five flavours for $\Lambda_{\overline{MS}}$ if $Q^2 > m_b^2$. At the BGF vertex we have used five flavours too because in the kinematic range of this analysis m_{ij}^2 is above $4 \cdot m_b^2$. Using four flavours at the BGF vertex in the PROJET program would increase the $\alpha_s(M_{Z^0})$ value by 0.0025. In the x, Q^2 region under study the contribution from massive $b-$quarks to the proton structure function is calculated to be below 2% [30].

8   Determination and Q^2 Dependence of α_s

The value of α_s was determined by varying $\Lambda_{\overline{MS}}^{(5)}$ in the QCD calculation until the best fit to the ratio R_{2+1} was obtained at $y_{cut} = 0.02$. The slope of the measured R_{2+1} as a function of y_{cut} agrees with that from the calculation, showing that the result is not sensitive to the particular value of y_{cut} used. We chose $y_{cut} = 0.02$ for the fit because the contribution from R_{3+1}, which is a higher order effect, becomes negligible for $y_{cut} \geq 0.02$. Furthermore the statistics are large and the jets are resolvable at this value and the 2-jet system has a large invariant mass.

Figures 2a–d show the corrected jet rates, R_{1+1}, R_{2+1} (also shown in Tab. 1) and R_{3+1} as a function of y_{cut} for data compared with the DISJET and PROJET NLO QCD calculations for the three Q^2 intervals and for the combined region. Only statistical errors are shown. All NLO terms are taken into account in both programs; however, they use different approximations for some of these terms. There is good agreement between the corrected jet rate and the NLO QCD calculation over most of the range in y_{cut} shown and in particular at the nominal $y_{cut} = 0.02$, where the α_s value was extracted for this analysis. Both programs agree well in their prediction of the jet-rate dependence as a function of y_{cut}. The best fit values for α_s are used in the calculation. The range in y_{cut} was restricted to 0.01 to 0.06 because at lower values of y_{cut} the jets are not experimentally resolvable and higher order corrections are significant, while at larger values terms proportional to y_{cut}, neglected in the calculation, become significant. Moreover, uncertainties in the renormalisation scale and the hadronisation corrections also become large for y_{cut} above ≈ 0.06 [27].

The values of α_s are plotted in Fig. 3 as a function of Q for each of the three Q^2 ranges. They are calculated from the fitted values of $\Lambda_{\overline{MS}}^{(5)}$. In Tab. 2 the α_s values determined for the three ranges in Q^2 as well as for the full kinematic range are listed. Also shown are the values of α_s extrapolated to $Q = M_{Z^0}$. Both statistical and systematic errors (discussed in the following section) are given.

In addition Fig. 3 shows the curves for $\Lambda_{\overline{MS}}^{(5)} = 100$, 200, and 300 MeV. The measured α_s decreases with increasing Q, consistent with the running of the strong coupling constant if Q^2 is taken as the scale. The fit to a running α_s (where α_s was determined in the full Q^2 range) yields a χ^2 of 2.2 for 2 degrees of freedom, which corresponds to a confidence level of 58.6%.

A least squares fit to the hypothesis of a constant α_s was performed. Only statistical errors were considered in this fit as the systematic errors are strongly correlated. This fit yields a χ^2 of 7.7 for 2 degrees of freedom, which corresponds to a confidence level of 2.1%. Taking into consideration the systematic uncertainties, the χ^2 for constant α_s varies from 4.4 (changing energy scale by -5%) to 10.3. A constant α_s is thus ruled out at 90% confidence level. The three values of α_s, expressed at the mass of the Z^0 boson, are consistent within the errors.

Q^2 (GeV^2)	$<Q>$ (GeV)	$\Lambda^{(5)}_{\overline{MS}}$ (MeV)	$\alpha_s(Q)$	$\alpha_s(M_{Z^0})$
$120 - 240$	13.3	$251\ ^{+108}_{-97}\ ^{+31}_{-74}\ ^{+115}_{-105}$	$0.171\ ^{+0.015}_{-0.017}\ ^{+0.005}_{-0.012}\ ^{+0.016}_{-0.018}$	$0.120\ ^{+0.007}_{-0.008}\ ^{+0.002}_{-0.006}\ ^{+0.007}_{-0.009}$
$240 - 720$	20.4	$217\ ^{+90}_{-74}\ ^{+76}_{-60}\ ^{+119}_{-67}$	$0.152\ ^{+0.011}_{-0.011}\ ^{+0.010}_{-0.009}\ ^{+0.014}_{-0.010}$	$0.117\ ^{+0.006}_{-0.007}\ ^{+0.006}_{-0.005}\ ^{+0.008}_{-0.006}$
$720 - 3600$	35.5	$86\ ^{+82}_{-58}\ ^{+30}_{-47}\ ^{+61}_{-24}$	$0.118\ ^{+0.013}_{-0.017}\ ^{+0.006}_{-0.012}\ ^{+0.010}_{-0.006}$	$0.103\ ^{+0.010}_{-0.013}\ ^{+0.004}_{-0.010}\ ^{+0.008}_{-0.004}$
$120 - 3600$	22.1	$208\ ^{+64}_{-53}\ ^{+57}_{-50}\ ^{+89}_{-75}$	$0.148\ ^{+0.008}_{-0.008}\ ^{+0.007}_{-0.007}\ ^{+0.011}_{-0.012}$	$0.117\ ^{+0.005}_{-0.005}\ ^{+0.004}_{-0.005}\ ^{+0.007}_{-0.007}$

Table 2: The measured values of $\Lambda^{(5)}_{\overline{MS}}$ and α_s for the three ranges in Q^2 as well as for the full Q^2 range. The first error is statistical, the second corresponds to the experimental systematic uncertainty and the third to the theoretical systematic uncertainties (hadronisation, parton density and scale uncertainty).

9 Systematic Uncertainties

9.1 Experimental, Hadronisation and Parton Density Effects

Sources of systematic uncertainties in the α_s determination were grouped into the following classes: event selection, energy scale, jet analysis, fitting method, model dependence of detector corrections, hadronisation corrections and parton density (see Fig. 4). The first five classes were attributed to the experimental systematic error. The uncertainties were studied for each of the three Q^2 ranges separately as well as for the combined kinematic region. Only the systematic uncertainty from the latter study is described here. To illustrate the systematic uncertainty in α_s associated with each systematic effect, the fitted α_s value obtained when the systematic effect is varied was compared with the central value of α_s (see Tab. 2).

The subgroups of experimental systematic errors are denoted by (a)-(e). The systematic errors from the event selection (a) included: effect of using a different electron finding algorithm; variations of the selection criteria, $E - P_Z > 45$ GeV; $y_e < 0.7$. The errors from the energy scale (b) included a $\pm 5\%$ error assigned to the uncertainty of the calorimeter energy response. The errors from the jet analysis (c) included: the choice of a different mass scale, $W^2_{DA} = s\,(1 - x_{DA})\,y_{DA}$ and $W^2_{JB} = s\,(1 - x_{JB})\,y_{JB}$, in the JADE scaled mass definition, $y_{ij} = m^2_{ij}/W^2$; the cells around the FCAL beam pipe, which contain mainly the proton remnant, were first preclustered and the resulting objects were used in the jet clustering algorithm (instead of the

cell vectors themselves). The errors from the fitting method (d) included: a QCD fit at y_{cut}=0.03 instead of y_{cut}=0.02; the analysis was cross-checked by a QCD fit to the differential jet rates, D_{1+1}, defined by $D_{1+1}(y_{cut}) = [R_{1+1}(y_{cut} + \Delta y_{cut}) - R_{1+1}(y_{cut})]/\Delta y_{cut}$; a more restrictive z-cut, $0.15 < z < 0.85$, was used. Finally, the error from the model dependence of the corrections for the detector acceptance and resolution (e) was estimated by using the colour-dipole model [31] as implemented in the ARIADNE 4.06 Monte Carlo [32]. The largest uncertainties for each subgroup were added in quadrature to give the experimental systematic error.

To evaluate the uncertainty of the hadronisation correction, several aspects of the hadronisation scheme were varied while the standard detector corrections based on the LEPTO MEPS Monte Carlo were retained. These studies were performed at the generator level. First, parameters in the Lund string fragmentation model [33] were varied: a in the 'symmetric fragmentation function', which regulates the longitudinal quark fragmentation, was varied between 0.1 and 1; σ_{Pt}, which controls the hadron transverse momentum distribution was varied between 0.25 and 0.45 GeV. Second, parameters of the parton shower model employed in the LEPTO MEPS Monte Carlo were changed: y_{min} was varied between 0.005 and 0.015; the minimum virtuality scale, Q_0, at which the parton showering is stopped, was changed from 0.8 to 4 GeV; the primordial transverse momentum k_T of the struck parton in the proton was varied from 0.44 to 0.7 GeV. Finally, a completely different hadronisation model as implemented in the HERWIG 5.8 Monte Carlo [34] was used. Most of these changes result in relatively small systematic errors in α_s as shown in Fig. 4. The two largest deviations from the central value of α_s arise from the change of the hadronisation model and from the variation of Q_0.

We also repeated the analysis with parton density sets MRSA, GRV HO, and CTEQ 3M in the NLO calculation, all of which describe the results from present DIS data well [16]. The differences in $\alpha_s(22.1 \text{ GeV})$ from the central value are small (< 0.0022), as shown in Fig. 4. The fitted α_s value depends only weakly on the α_s value used in the parton density parametrisations [26].

In the x, Q^2 region under study the contribution from massive $b-$quarks to the proton structure function is calculated to be below 2% [30]. The effect of calculating with four instead of five flavours at the BGF vertex was estimated with the PROJET program and was found to increase $\alpha_s(M_{Z^0})$ by 0.0025. This number is not included in the systematic errors given.

9.2   Scale Dependence Effects

Our best estimate of the scale uncertainty in the measured α_s was obtained from DISJET and PROJET by varying μ_R and μ_F from $0.4 \ Q^2$ to $2.0 \ Q^2$, redoing the fit to the jet rates and evolving to obtain the corresponding value of α_s at the original scale Q (shown in Fig. 4 for the full Q^2 range). The scale dependence decreases with increasing Q and becomes negligible in the highest Q^2 interval. It is slightly larger in DISJET than in PROJET.

Deep inelastic production of jets is a multi-scale process and it is not evident that Q^2 is the best choice [4, 35] for the renormalisation and factorisation scales in the perturbative calculation. Alternative scales have been suggested, e.g. p_T^2 of the jets or the square of the invariant mass, m_{ij}^2, of the two jets. As a simple test the ratios $< p_T^2/Q^2 >$ and $< m_{ij}^2/Q^2 >$ were evaluated for the full Q^2 range for 2+1 jet events and were used to estimate the resultant change of scale and hence of the uncertainty in α_s. For our events these ratios typically lie between 0.4 and 2,

i.e. within the range explored above in our estimation of the scale uncertainty using DISJET and PROJET.

For each group in Fig. 4 we quote the largest deviation from the central value in each direction as the systematic error. The positive and negative deviations are then added in quadrature separately to give the systematic error. The total systematic uncertainty for the value of α_s resulting from the effects studied in Fig. 4 is comparable to the statistical errors. In the final result given below the uncertainties from the experimental and theoretical systematic effects (hadronisation, parton density distributions and scale effects) are quoted separately.

10 Summary

Multi-jet production in ep collisions was investigated using the JADE jet definition. In ep collisions the application of the single jet resolution parameter, y_{cut}, is not sufficient to restrict the phase space of 2+1 jet production to an experimentally well understood and theoretically safe region. An additional cut on the parton variable z is introduced, which excludes the problematic region where higher order effects are important and jets are not well measured in the experiment. With this additional cut the multi-jet production rate in DIS is well reproduced by $\mathcal{O}(\alpha_s{}^2)$ perturbative QCD calculations.

The value of $\alpha_s(Q)$ was determined in three Q^2 regions in a single experiment and was found to decrease with Q, consistent with the running of the strong coupling constant.

The value for α_s using the data from the entire kinematic range $120 < Q^2 < 3600$ GeV^2, and expressed at the Z^0 mass is given by:

$$
\begin{aligned}
\alpha_s(M_{Z^0}) &= 0.117 \pm 0.005 \,(stat) \,^{+0.004}_{-0.005}\,(exp) \,^{+0.005}_{-0.004}\,(had) \,^{+0.001}_{-0.001}\,(pd) \,^{+0.005}_{-0.006}\,(scale) \\
&= 0.117 \pm 0.005 \,(stat) \,^{+0.004}_{-0.005}\,(syst_{exp}) \,\pm 0.007 \,(syst_{theory}),
\end{aligned}
$$

where $stat$ corresponds to the statistical error and the systematic error components ($syst$) consist of the experimental (exp), hadronisation (had), parton density (pd) and the scale ($scale$) related uncertainties. The overall systematic error is separated into its experimental (exp) and theoretical ($theory$) contribution.

Our value of α_s is consistent with the most recent compilation by the Particle Data Group [36] of previous measurements of $\alpha_s(M_{Z^0})$ using different methods: 0.112 ± 0.005 (DIS), 0.121 ± 0.006 (e^+e^- event shape analysis) and 0.124 ± 0.007 (Z^0 width). The good agreement between our value of α_s and the results obtained using other methods in different kinematic regimes represents a significant test of QCD.

Acknowledgements

References

[1] D. Graudenz, Phys. Lett. B256 (1991) 518.

[2] T. Brodkorb and J.G. Körner, Z. Phys. C54 (1992) 519.

[3] D. Graudenz, Phys. Rev. D49 (1994) 3291.

[4] T. Brodkorb and E. Mirkes, Z. Phys. C66 (1995) 141.

[5] JADE Collab., W. Bartel et al., Z. Phys. C33 (1986) 23;
    JADE Collab., S. Bethke et al., Phys. Lett. B213 (1988) 235.

[6] E665 Collab., M. Adams et al., Phys. Rev. Lett. 69 (1992) 1026;
    E665 Collab., M. Adams et al., Phys. Rev. Lett. 72 (1994) 466.

[7] ZEUS Collab., M. Derrick et al., Phys. Lett. B306 (1993) 158.

[8] H1 Collab., I. Abt et al., Z. Phys. C61 (1994) 59.

[9] ZEUS Collab., M. Derrick et al., Z. Phys. C67 (1995) 81.

[10] H1 Collab., T. Ahmed et al., Phys. Lett. B346 (1995) 415.

[11] ZEUS Collab., M. Derrick et al., Phys. Lett. B293 (1992) 465;
     The ZEUS Detector, Status Report 1993, DESY 1993.

[12] C. Alvisi et al., Nucl. Instr. and Meth. A305 (1991) 30.

[13] N. Harnew et al., Nucl. Instr. and Meth. A279 (1989) 290;
     B. Foster et al., Nucl. Phys. B (Proc. Suppl.) 32 (1993) 181;
     B. Foster et al., Nucl. Instr. and Meth. A338 (1994) 254.

[14] A. Andresen et al., Nucl. Instr. and Meth. A309 (1991) 101;
     A. Caldwell et al., Nucl. Instr. and Meth. A321 (1992) 356;
     A. Bernstein et al., Nucl. Instr. and Meth. A336 (1993) 23.

[15] K.H. Streng, T.F. Walsh and P.M. Zerwas, Z. Phys. C2 (1979) 237;
     J.G. Körner, E. Mirkes, and G.A. Schuler, Int. J. Mod. Phys. A4 (1989) 1781.

[16] ZEUS Collab., M. Derrick et al., Z. Phys. C65 (1995) 379.

[17] F. Jacquet and A. Blondel, Proceedings of the study for an ep facility for Europe, DESY
     79/48 (1979) 391.

[18] T. Brodkorb, J.G. Körner, E. Mirkes, G.A. Schuler, Z. Phys. C44 (1989) 415.

[19] D. Graudenz, N. Magnussen, Proceedings of the HERA Workshop 1991 at DESY, eds.
     W. Buchmüller, G. Ingelman.

[20] G. Ingelman, LEPTO, version 6.1, Proc. 'Physics at HERA', W. Buchmüller, G. Ingelman
     (eds.), DESY Hamburg 1992, vol. 3, p.1366.

[21] B. Andersson et al., Phys. Rep. 97 (1983) 31;
T. Sjöstrand and M. Bengtsson, Comp. Phys. Comm. 43 (1987) 367.

[22] H. Spiesberger, DJANGO6, version 2.1, unpublished program manual (1995); version 1.1 is described in K. Charchuła, G.A. Schuler and H. Spiesberger, Comp. Phys. Commun. 81 (1994) 381.

[23] H. Spiesberger, HERACLES, version 4.5, unpublished program manual (1995); version 4.0 is described in A. Kwiatkowski, H.-J. Möhring and H. Spiesberger, Comp. Phys. Commun. 69 (1992) 155.

[24] GEANT 3.13: R. Brun et al., CERN DD/EE-84-1 (1987).

[25] A.D. Martin, W.J. Stirling and R.G. Roberts, Phys. Lett. B306 (1993) 145.

[26] A. Vogt, Phys. Lett. B354 (1995) 145;
A.D. Martin, W.J. Stirling and R.G. Roberts, DTP/95/48 (1995).

[27] G. Ingelman and J. Rathsman, Z. Phys. C63 (1994) 589.

[28] T. Brodkorb and E. Mirkes, Univ. of Wisconsin, MAD/PH/821 (1994).

[29] D. Graudenz, CERN-TH.7420/94 (1994), to appear in Comp. Phys. Comm.

[30] E. Laenen, S. Riemersma, J. Smith and W.L. van Neerven, Nucl. Phys. B392 (1993) 228;
S. Riemersma, J. Smith and W.L. van Neerven, Phys. Lett. B347 (1995) 143;
M. Glück, E. Reya, M. Stratmann, Nucl. Phys. B422 (1994) 37;
A. Vogt, Workshop on Proton, Photon and Pomeron Structure, Durham, September 1995.

[31] B. Andersson et al., Z. Phys. C43 (1989) 625.

[32] L. Lönnblad, Z. Phys. C65 (1995) 285.

[33] T. Sjöstrand, CERN-TH 7112 (1993).

[34] G. Marchesini et al., Comp. Phys. Comm. 67, (1992) 465.

[35] A.D. Martin, W.J. Stirling and R.G. Roberts, Phys. Lett. B266 (1991) 173.

[36] Particle Data Group, L. Montanet et al., Phys. Rev. D50 (1994).
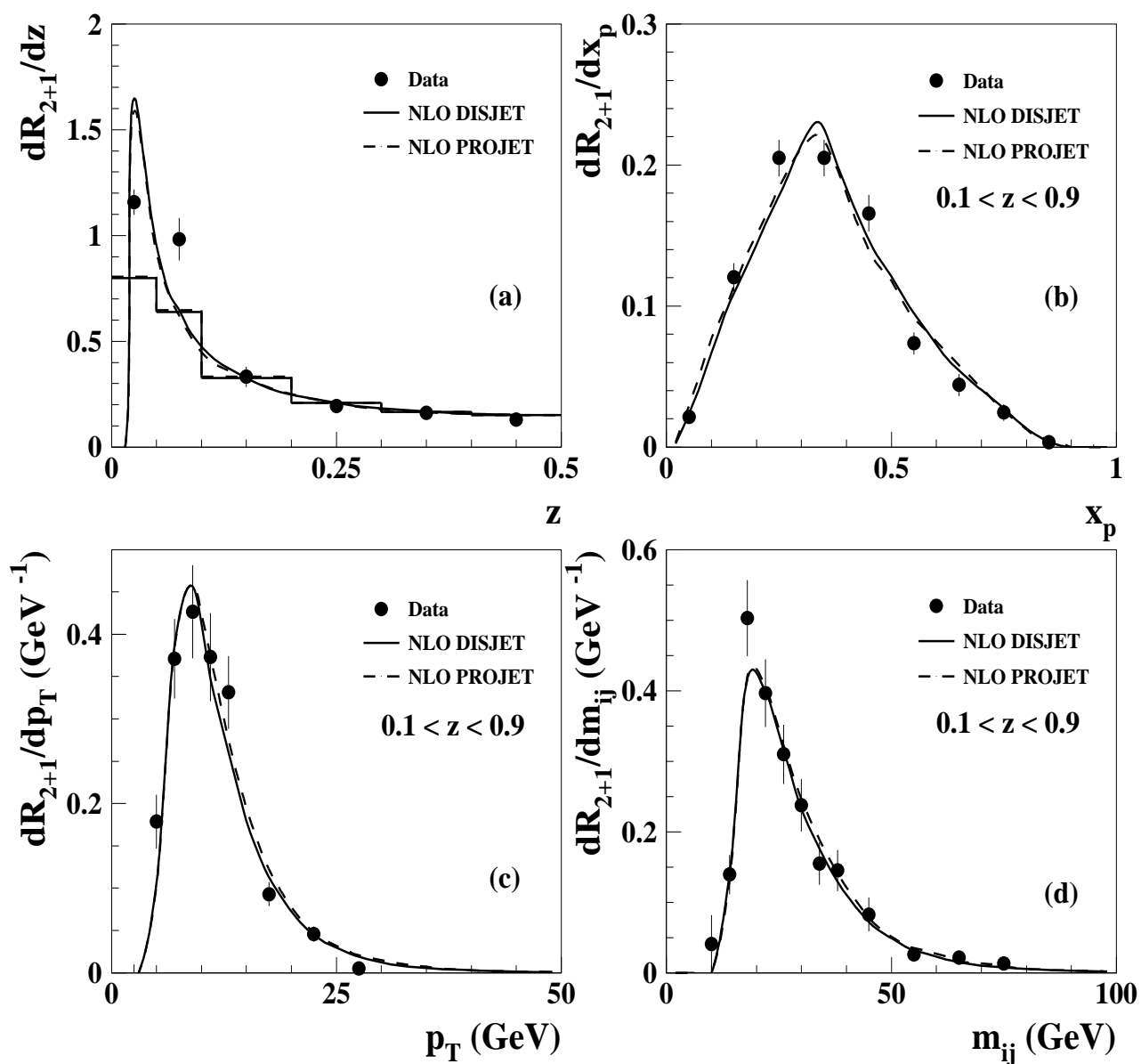
ZEUS 1994

Figure 1: (a) Distribution of the parton variable, z, of one of the two non-remnant jets in 2+1 jet events in the range $120 < Q^2 < 3600$ GeV^2, compared to the NLO calculations (PROJET and DISJET). The dots with error bars are the measured data. The curves represent the theoretical predictions after the application of the cuts. The histograms show the same theoretical prediction with the binning of the data. (b) Distribution of x_p for 2+1 jet events. (c) Transverse momentum distribution p_T for the two jets. (d) Invariant mass distribution m_{ij} of the two non-remnant jets. Only events satisfying $0.1 < z < 0.9$ were plotted in Figs. b–d. All jet rates are evaluated for $y_{cut} = 0.02$. The data points are corrected to the parton level and plotted with their statistical errors only.
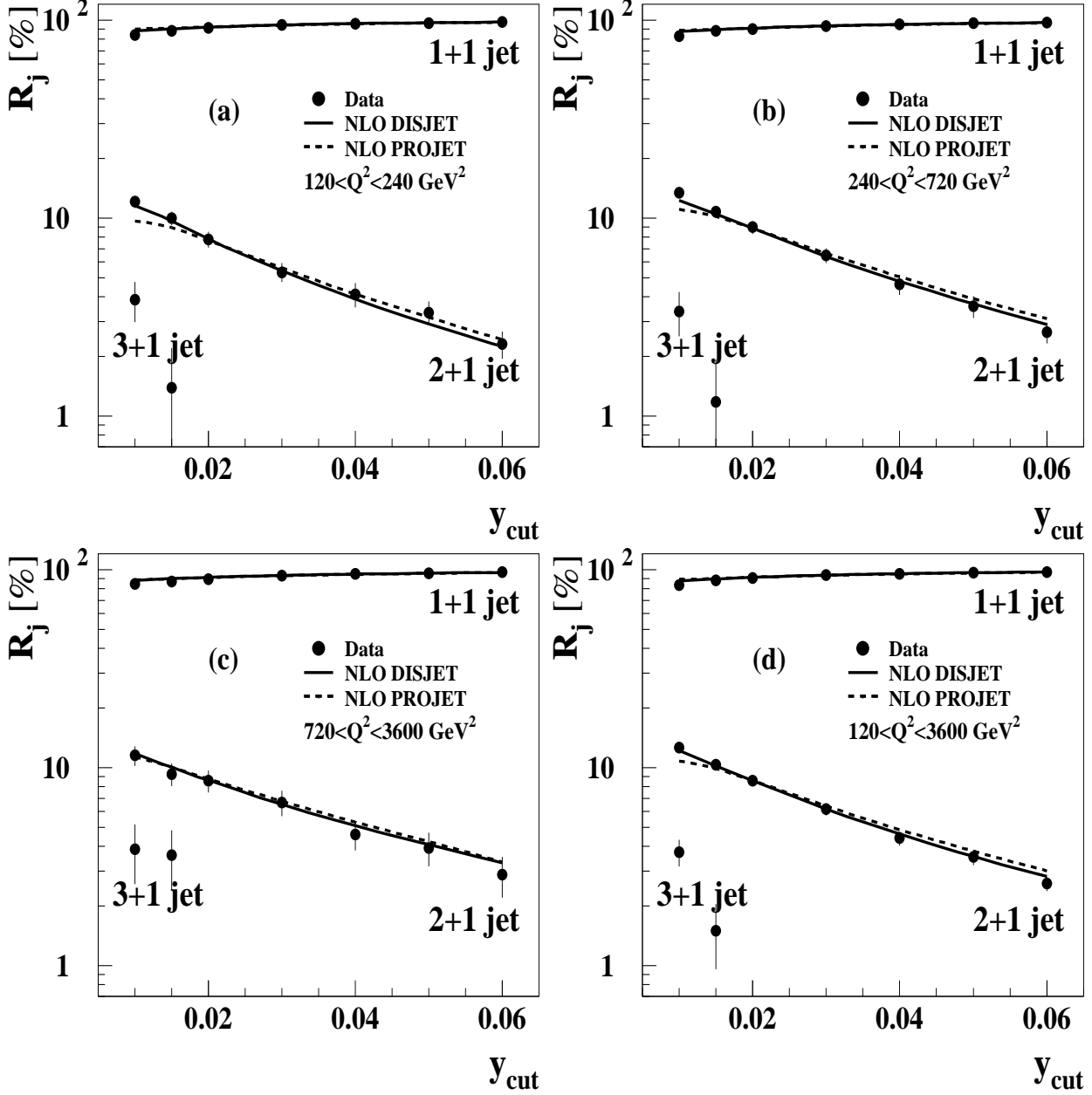
ZEUS 1994

Figure 2: Jet production rates R_j as a function of the jet resolution parameter y_{cut} for Q^2 in the range (a) $120 < Q^2 < 240$ GeV^2, (b) $240 < Q^2 < 720$ GeV^2, (c) $720 < Q^2 < 3600$ GeV^2, and (d) $120 < Q^2 < 3600$ GeV^2. Only statistical errors are shown. Two NLO QCD calculations, DISJET and PROJET, each with the value of $\Lambda_{\overline{MS}}$ obtained from the fit at y_{cut}=0.02, are also shown.
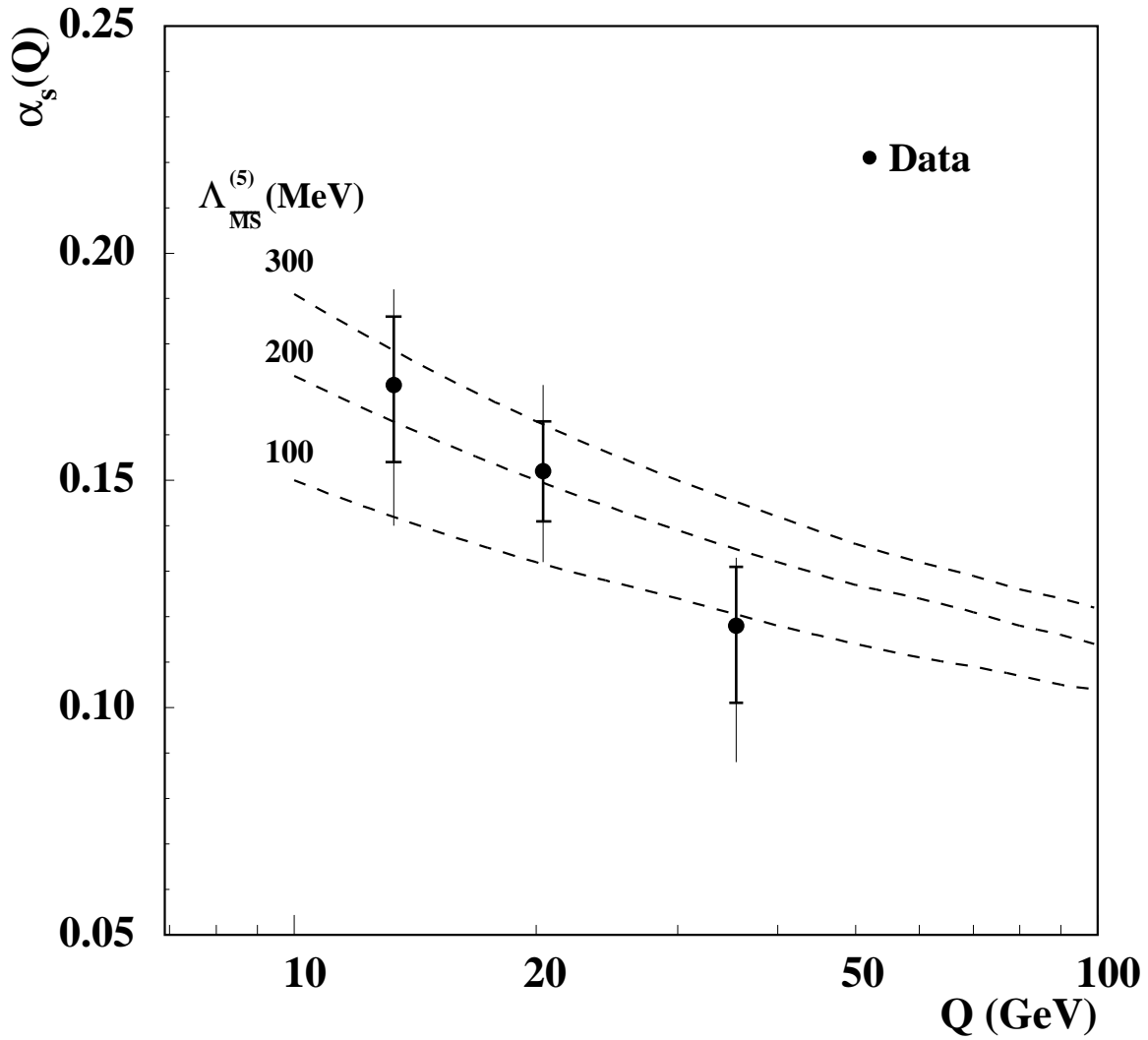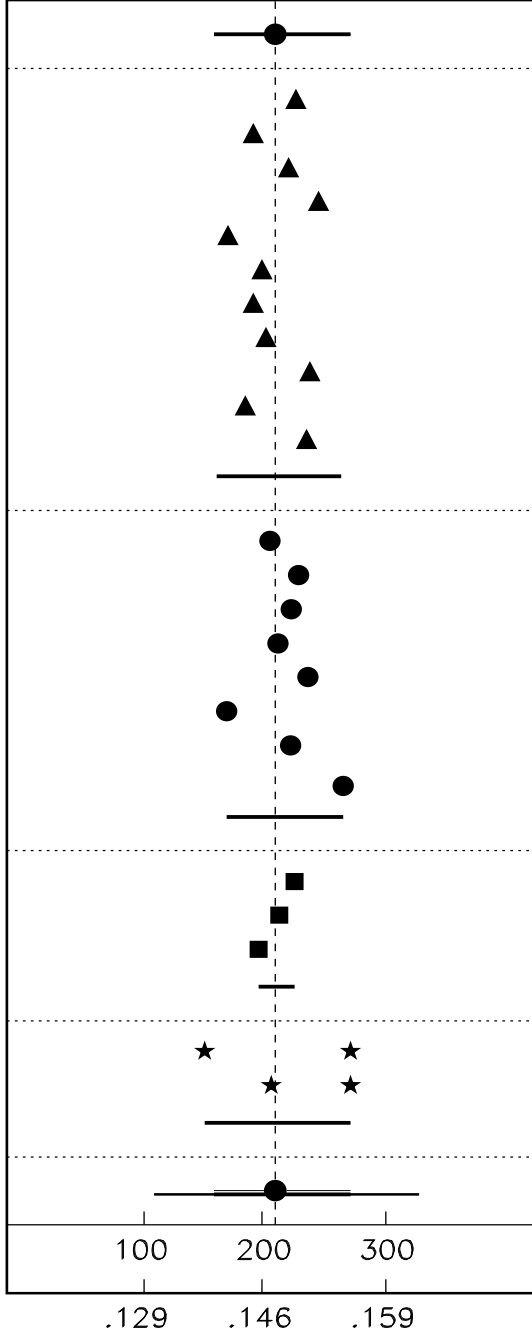
Figure 3: Measured values of $\alpha_s(Q)$ for three different Q^2 regions. The statistical error corresponds to the inner bar and the thin bar reflects the statistical and systematic error added in quadrature. Note that the systematic errors are strongly correlated. The dashed curves represent α_s with $\Lambda^{(5)}_{\overline{MS}} = 100$, 200, and 300 MeV.

Statistical Error

(a) { Electron finder
     E−P$_z$ > 45 GeV
     y$_e$ < 0.7

(b) { Energy scale (+5%)
     Energy scale (−5%)

(c) { Method of W calculation
     Preclustering of cells

(d) { y$_{cut}$ dependence
     Differential jet rate method
     0.15<z<0.85

(e)   Detector correction(ARIADNE)

Experimental Systematics

a=0.1 } Fragmentation parameter
a=1.0

σ$_{Pt}$=0.25 GeV } σ$_{Pt}$ of fragmentation
σ$_{Pt}$=0.45 GeV   function

y$_{min}$=0.015   Minimum y$_{ij}$ of parton in ME
Q$_0$=4 GeV   Minimum PS virtuality
k$_t$=0.7 GeV   Intrinsic k$_t$ of struck parton
Herwig cluster hadronisation

Hadronisation Correction

MRSA
GRV HO
CTEQ3M

Parton Density Uncertainty

$0.4<x_\mu^R=x_\mu^F=\mu^2/Q^2<2.0$ (DISJET)
$0.4<x_\mu^R=x_\mu^F=\mu^2/Q^2<2.0$ (PROJET)

Scale Uncertainty

Total Error

$\Lambda\frac{(5)}{\overline{MS}}$ (MeV)

α_s(Q=22.1 GeV)

100   200   300

.129   .146   .159

Figure 4: Systematic uncertainties in the measured value of α_s (and $\Lambda\frac{(5)}{\overline{MS}}$) for Q^2 in the range $120 < Q^2 < 3600$ GeV^2 expressed as the deviation from the central value for the listed alterations in the analysis. Sources of systematic uncertainties are grouped into the four areas: experiment, hadronisation correction, parton density, and scale. The experimental uncertainty is subdivided into: (a) event selection, (b) energy scale, (c) jet analysis, (d) fitting method, and (e) model dependence of the detector correction.